Quantum Chemical Modeling of Reaction Mechanism for 2-Oxoglutarate Dependent Enzymes: Effect of Substitution of Iron by Nickel and Cobalt

Igor A. Topol*,[†] Alexander V. Nemukhin,[‡,§] Konstantin Salnikow,[||] Raul E. Cachau,[†] Yuri G. Abashkin,[†] Kazimierz S. Kasprzak,[||] and Stanley K. Burt[†]

Advanced Biomedical Computing Center, SAIC Frederick, National Cancer Institute at Frederick, Frederick, Maryland 21702, Department of Chemistry, M. V. Lomonosov Moscow State University, Moscow, 119992, Russia, Institute of Biochemical Physics, Russian Academy of Sciences, Moscow, 119997, Russia, and Laboratory of Comparative Carcinogenesis, National Cancer Institute at Frederick, Frederick, Maryland 21702

Received: October 3, 2005; In Final Form: January 6, 2006

Enzymatic hydroxylation reactions carried out by 2-oxoglutarate (2OG) dependent iron-containing oxygenases were recently implicated in oxygen sensing. In addition to oxygen depletion, two metals, cobalt and nickel, are capable of inducing hypoxic stress in cells by inhibiting oxygenase activity. Two possible scenarios have been proposed for the explanation of the hypoxic effects of cobalt and nickel: oxidation of enzyme-bound iron following cobalt or nickel exposure, and substitution of iron by cobalt or nickel. Here, by using density functional theory calculations, we modeled the reaction route from the reaction components to the high-spin metal−oxide intermediate in the activation of oxygen molecule by 2OG-dependent enzymes for three metal ions Fe(II), Ni(II), and Co(II) in the active site. An initial molecular model was constructed based on the crystal structure of iron-containing asparaginyl hydroxylase (FIH-1). Nickel- and cobalt-containing enzymes were modeled by a consequent replacement of the iron in the active center. The energy profiles connecting stationary points on the potential surfaces were computed by using the intrinsic reaction coordinate (IRC) technique from the located transition states. The results of calculations show that the substitution of iron by nickel or cobalt modifies the reaction energy profile; however, qualitatively, the reaction mechanism remains essentially the same. Thus, we would postulate that if the iron ion in the active site were substitutable by nickel and/or cobalt ions enzyme activity would be considerably altered due to high activation barriers.

Introduction

2-Oxoglutarate (2OG) dependent iron-containing oxygenases have recently attracted attention since four members of this family namely, the prolyl-4-hydroxylase domain proteins (PHD1−3) and asparaginyl hydroxylase (FIH-1), are implicated in cellular oxygen sensing.[1−3] Hydroxylation of HIF-α subunit of hypoxia inducible transcription factor (HIF-1) in the presence of oxygen, and 2OG at either of two conserved prolyl residues, enables its recognition by the von Hippel-Lindau tumor suppressor protein, which targets it for proteasomal degradation. Hydroxylation of an asparaginyl residue in the C-terminal transactivation domain of HIF-α directly prevents its interaction with the transcriptional coactivator p300.[4] Since HIF-1 transcription factor is a key regulator of angiogenesis and maintenance of oxygen balance in tissues, the studies of structure, function, and mechanism of action of 2OG-dependent iron-containing oxygenases are of special importance for biochemical and medical applications including cardiovascular disease and cancer.[4,5] It has been demonstrated that exposure of cells to Ni(II) or Co(II) at moderate to low concentrations causes a response very similar to that observed during hypoxia.[4] Recently, we have shown that the depletion of cellular ascorbate following Ni(II) or Co(II) exposure is, in part, responsible for the inhibition of HIF-α hydroxylation.[6] These data emphasize an important role of ascorbate in maintaining enzyme-bound iron in state II. However, in addition to ascorbate depletion, an iron substitution by Ni(II) or Co(II) in the active sites may also be the cause of hypoxia-like response when these ions are present. All three metal ions, iron, nickel, and cobalt can be part of naturally occurring non-heme oxygenases where they can be enzymatically active.[7,8] It is not known, however, whether 2OG-dependent iron-containing oxygenases will be more or less reactive with the substitution of iron with Ni(II) or Co(II).

This paper aims to verify computationally how the reaction path

$$\mathrm{M(II)} + \mathrm{O_2} + \text{2-oxoglutarate} \rightarrow \mathrm{MO} + \mathrm{CO_2} + \text{succinate}$$

depends on the nature of the metal (M = Fe, Ni, Co) in the active site of the enzyme. To this end, quantum chemical calculations have been carried out at the density functional theory (DFT) level for the molecular cluster constructed on the base of the crystal structure of iron-containing hypoxia-inducible factor asparaginyl hydroxylase, or FIH.[9] This non-heme enzyme contains an iron(II) center that is coordinated by two histidines, one aspartate, and the 2OG species bound through its C-1 carboxylate and C-2 carbonyl moieties. The crystal structure of FIH with 2OG and a substrate obtained under anaerobic conditions and solved at the resolution 2.25 Å has been recently reported (Protein Data Bank (PDB) ID: 1H2L).[10] This structure provided us a reasonable starting arrangement of atoms in the ligand shell around iron in the native enzymatic system.

[†] SAIC Frederick, National Cancer Institute at Frederick.
[‡] M. V. Lomonosov Moscow State University.
[§] Russian Academy of Sciences.
[||] Laboratory of Comparative Carcinogenesis, National Cancer Institute at Frederick.

10.1021/jp055633k CCC: $33.50
Published on Web 03/03/2006

When considering the mechanism of the 2OG-dependent oxygenases, it is a general belief[11] that binding of O_2 to the sixth available position in the coordination environment produces the Fe(III)−superoxo species that attacks the 2OG carbonyl group, leading to decomposition of 2OG and heterolytic O−O bond cleavage. The resulting Fe(IV)═O species is capable of inserting oxygen into the target C−H bond of the substrate.[11,12]

Previous quantum chemical calculations performed to characterize quantitatively the reaction mechanism of 2OG-dependent non-heme enzymes were described by Borowski, Bassan, and Siegbahn.[13,14] These authors considered a molecular complex that modeled the active site of another enzyme from the 2OG-dependent oxygenase group, clavaminic acid synthase.[13] They used density functional theory (DFT) calculations to construct the energy profile for chemical transformations occurring within the 62-atom cluster. The results of these calculations support the mechanism in which all chemical transformations occur on a quintet potential energy surface, and the sequence of events corresponds to a stepwise procedure: the C−C bond in 2OG is broken, generating the iron−peracid complex and CO_2 (step 1), and then the O−O bond heterolysis leads to the active ferryl−oxo intermediate (step 2). In published calculations constrained geometry optimizations were performed with a valence double-ζ basis set coupled with an effective core potential for iron (the LACVP option). For the optimized structures the electronic energy was computed with a bigger basis set of triple-ζ quality with polarization functions on all atoms (LACV3P**). The solvent corrections were introduced by using the continuum model with the dielectric constant of 4. The imposed constraints during geometry optimization intended to fix positions of the outermost atoms in the molecular cluster according to the known X-ray structure of the enzyme−2OG complex in the absence of oxygen. The possible energy errors due to such constraints were estimated to be less than 2 kcal/mol. The energy of the active site−O_2 complex in the triplet state was used as a reference point for the energy diagram due to tentative estimates of possible effects not covered by the model. According to the calculation results, the rate-limiting stage is formation of the iron(II)−peracid complex coupled with decarboxylation of 2OG (step 1). The activation energy (the energy difference between the top of the potential in the quintet state and the reagents in the triplet state) was computed to be 16.1 kcal/mol, while the overall energy effect of this stage was −41.1 kcal/mol. Then the CO_2 species was excluded from the model and the O−O bond cleavage was simulated within the rest of the cluster. It was found that the second step of the reaction proceeded through two transition states on a very flat potential energy surface, and the highest activation barrier along this fragment of the path was found to be 4.3 kcal/mol.

In a related paper, Borowski, Bassan, and Siegbahn modeled the reaction energy profile for dioxygen activation by the biomimetic complex Fe[(hydrotris(3,5-diphenylpyrazol-1-yl)-(benzoylformate)] using B3LYP calculations. They concluded that the biomimetic reaction proceeded "partially on the septet and partially on the quintet potential energy surface".[14] The septet and triplet states competed for the lowest energy structures, while the quintet state energy was considerably higher. Another paper[15] by the same authors described the results of similar studies of the reaction mechanism of 4-hydroxyphenylpyruvate dioxegenase, however, with the major emphasis on the finalizing stage of the reaction, showing that the initial phase (oxidative decarboxylation of 2OG) was essentially the same as presented in ref 13. In the above-mentioned work[15] no constraints for the optimization procedures were used.

Our computational approach, B3LYP/LANL2DZdp, is essentially the same as that used by Borowski, Bassan, and Siegbahn.[13] However, we did not impose geometry constraints in geometry optimizations, which allowed us to truly characterize minimum energy and transition state structures following the unconstrained vibrational analysis. Comparison of the computed positions of the ligands (His, Asp, 2OG) relative to iron with those in the X-ray structure showed that the reference crystal arrangement remained virtually intact. Another distinction from the model described in ref 13 is that we do not exclude the leaving group (CO_2) at any stages of simulations.

After the calculations of the energy profile for the iron-containing model were completed, we substituted Fe(II) by Ni(II) and Co(II), respectively, in the active center and repeated the calculations. Comparison of the three energy diagrams for the reaction path allowed us to assess possible effects of the metal center substitution in the active site.

Results of Calculations for the Iron Site

Starting from the relevant crystal structure (PDBID: 1H2L[10]), the model system, (composed of the iron ion, side chains of His199, His279, and Asp201 residues, a simplified 2OG species, and O_2) has been constructed. Equilibrium geometry configurations of all stationary points on potential energy surfaces have been fully optimized by using the B3LYP methodology and a slightly modified LANL2DZdp basis set (diffuse functions have been kept on oxygen atoms only) and the corresponding pseudopotential on the metal.[16] Calculations have been carried out by using the Gaussian 03 program system.[17] Several spin states compete for the ground electronic state of the system. The lowest energy configuration of the initial metal site−oxygen complex corresponds to $S = 3$ (septet); next follows the state with $S = 1$ (triplet), which is 7.7 kcal/mol higher in energy, and $S = 2$ (quintet), which is 10.7 kcal/mol higher with respect to $S = 3$. Several equilibrium geometry configurations for the metal site−O_2 molecule could be located on the potential energy surfaces of different spin states differing in energy and in relative orientation of the ligands.

As follows from several DFT calculations of the energy profiles for the reactions of oxygen activation by non-heme biomimetic complexes,[13,18] as well as from our calculations, immediately in the entrance channel there should be a change in the spin state of the system from septet ($S = 3$) to quintet ($S = 2$). Therefore, the results obtained for the quintet surface only are shown below.

To avoid ambiguities in the reference geometry configuration of the reagents, a reference structure was selected as follows. After the configuration corresponding to the first transition state (TS1) on the reaction route was located, the intrinsic reaction coordinate (IRC) calculations in the backward and forward modes arriving at the minimum energy configurations referring to the reagents (first minimum, M1) and to the reaction intermediate (second minimum, M2) were performed. The M1 structure, with all real vibrational frequencies serving as a reference point for the entire energy diagram, is shown in Figure 1.

Figure 1 shows the distances between the iron ion and the closest atoms of its ligands obtained in calculations and in the experimental studies of the crystal structure (PDBID: 1H2L[10]) of the enzyme without the oxygen molecule. As one can see, the calculation procedure results in a fairly accurate representation of the experimental entities. It is also clear that insertion

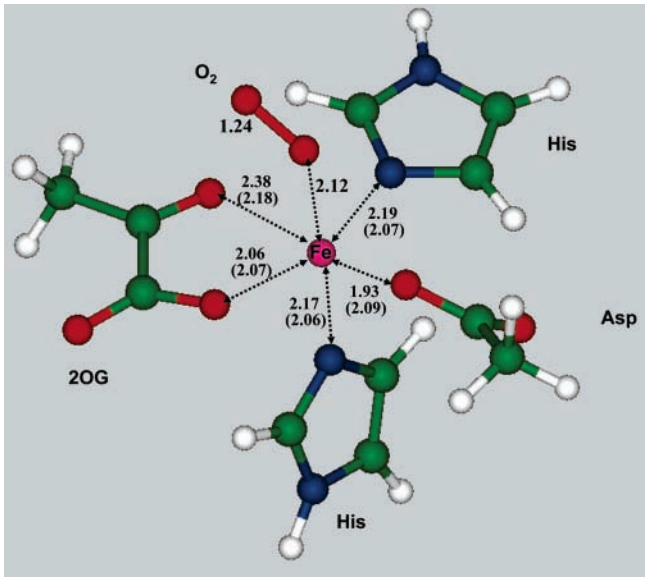

Figure 1. Equilibrium geometry configuration of the oxygen molecule−iron site complex (M1) in the quintet spin state, computed as the bottom of the downhill way from the first transition state TS1 toward the reagents. The distances in angstroms shown from iron to the atoms of the ligands are compared to those measured in the crystal structure 1H2L[10] of the enzyme without dioxygen (values in parentheses).

of the oxygen molecule inside the cavity does not considerably disturb the arrangement of atoms around the metal site. As seen in Figure 1, the oxygen molecule binds to the iron ion in the end-on mode and plays the role of the sixth ligand in the coordination of iron shell.

It is also instructive to compare this configuration (Figure 1) to that shown in Figure 3 of ref 13 for a somewhat larger biomimetic complex, also in the quintet spin state. The latter complex[13] is composed of the iron ion, oxygen molecule, simplified side chains of two His and Glu residues, simplified 2OG species in the same fashion as in our work, and simplified side chains of Tyr and Arg. That picture shows a similar structure with the end-on mode of oxygen binding to iron, with a close distance (2.09 Å vs 2.12 Å in our structure (Figure 1)) from proximal oxygen atom to iron. However, the O−O bond length, as shown in Figure 3 of ref 13, is 1.34 Å vs 1.24 Å in our structure (Figure 1). The elongated oxygen−oxygen bond distance (1.34 Å), typical for negative ion O_2^-, is a clear indication that at least partial electron transfer from iron to oxygen has occurred. Most likely, some disagreement obtained in two similar DFT calculations for similar molecular models with respect to such an important property of the metal site−oxygen complex as iron−oxygen charge transfer results from the presence of extra molecular groups (simplified side chains of Tyr and Arg) in the model of ref 13.

Figure 2 shows the structure of the first transition state (TS1) connecting the point of the reagents M1 and the point of the second local minimum corresponding to the reaction intermediate M2. This is a true transition state configuration with a single imaginary frequency of 416i cm^{-1}. As illustrated by bold black arrows in Figure 2, showing the dominant normal-mode vibrations, this frequency apparently refers to the route leading to insertion of oxygen to 2OG. The intermediate M2, shown as an inset in Figure 2, corresponds to the structure with a new C (from 2OG)−O (from O_2) bond.

Figure 3 illustrates the structure of the second transition state (TS2) on the reaction route. The only imaginary frequency (474i cm^{-1}) at this point apparently refers to the cleavage of the C−C

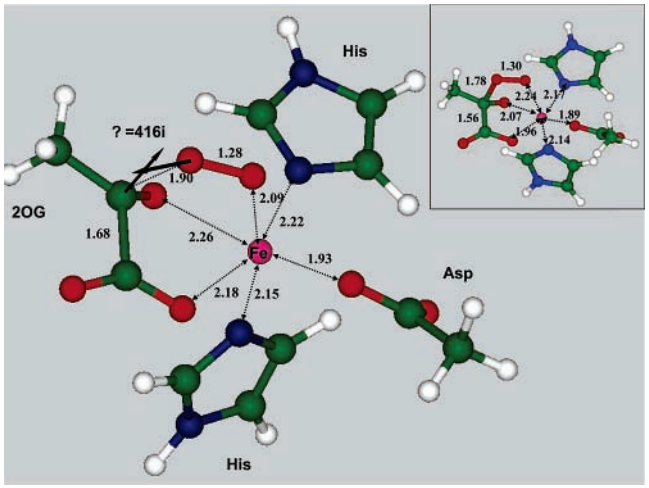

Figure 2. Geometry configuration of the first transition state TS1. Distances are given in angstroms. Bold black arrows show the principal displacements of atoms with the single imaginary frequency of 416i. The inset shows the structure of the M2 stationary point.

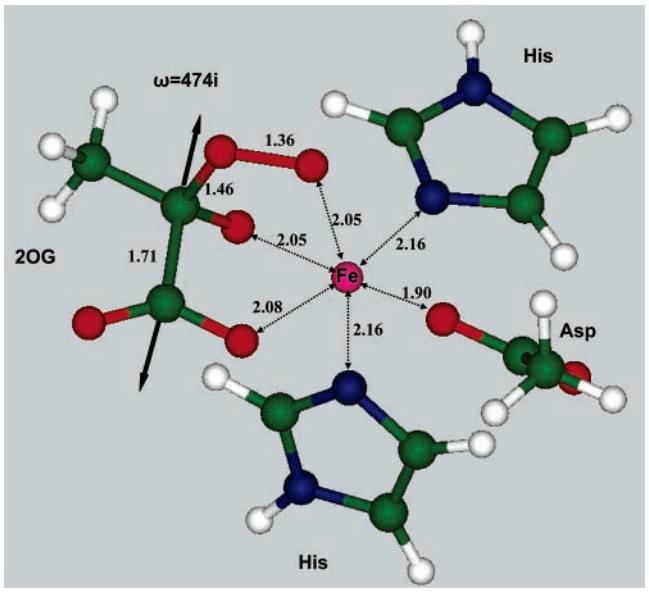

Figure 3. Geometry configuration of the second transition state TS2. Distances are given in angstroms. Bold black arrows show the principal displacements of atoms with the single imaginary frequency of 474i.

bond in 2OG after binding of oxygen to the latter. Therefore, by our calculations, the oxidative decarboxylation and formation of the ferrous−peracid complex occurs in two steps: (i) binding of activated O_2 to 2OG and (ii) decomposition of 2OG. As seen in Figure 4 of ref 13, the optimized structure for the quintet transition state, which is the only barrier found in ref 13 for this part of the reaction route, resembles our TS2: the O−O distance in O_2 is 1.39 Å (vs 1.36 Å in TS2), O (from O_2)−C (from 2OG) is 1.51 Å (vs 1.46 Å in TS2), the C−C distance in 2OG is 1.72 Å (vs 1.71 Å in TS2), and Fe−O (from O_2) is 2.33 Å (vs 2.05 Å in TS2). For some reason, the structure corresponding to TS1 in our calculations has not been located in ref 13.

Figure 4 shows the minimum energy configuration obtained following the IRC calculations from TS2 toward products, which we denote as M3. In these calculations structures similar to those described in Figure 5 of ref 13 for the iron−peracid−CO_2 complex have been obtained.

The next stage of the reaction is the cleavage of the O−O bond in the O_2 unit. Our calculations predict only one transition

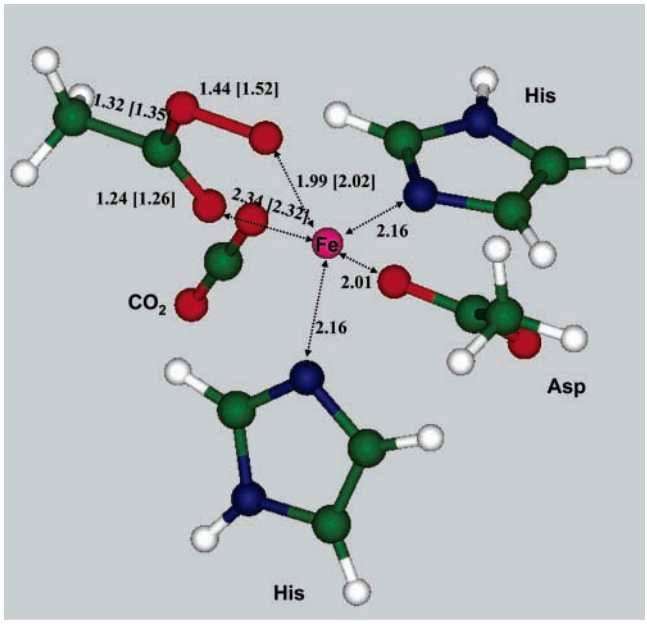

Figure 4. Computed structure of the reaction intermediate M3. The distances are given in angstroms, and the values in brackets correspond to the results of calculations of ref 13.

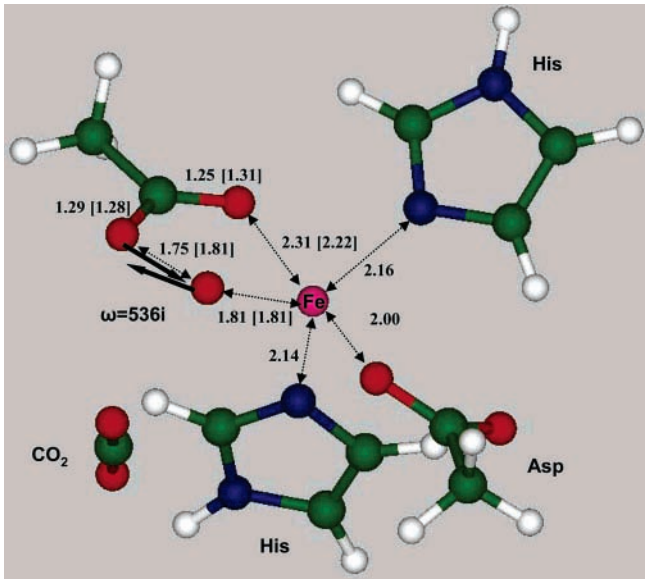

Figure 5. Computed structure of the third transition state TS3. Distances (in angstroms) without brackets are obtained in this work, and the values in brackets refer to the data in Figure 7 of ref 13.

state structure on the way from M3 to the ferryl−oxo complex with a short Fe−O bond, M4. In ref 15 for this stage of reaction also only one transition state was found. However, it should be noted that Borowski, Bassan, and Siegbahn reported two TS structures on this path of the reaction.[13] The structures of the third transition state T3 and of the final complex M4 are shown in Figures 5 and 6, respectively.

Comparison of these molecular complexes with the structures shown in Figures 7 and 10 of ref 13 allows us to conclude that the calculations performed for the iron-containing metal site resulted in the same destination point as previously reported.[13]

The computed energy diagram is illustrated in Figure 7. These energy values are comparable to those given in Figure 11 of ref 13, although there are some qualitative differences in the two calculations. Namely, the previous model predicts a single transition state (resembling our TS2) for the decarboxylation

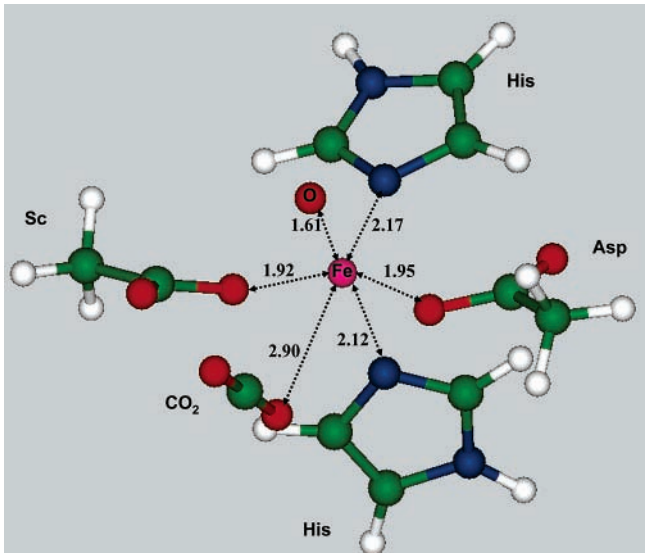

Figure 6. Structure of the complex (M4) with the active Fe−O unit. The short (1.61 Å) distance between iron and oxygen may be compared with the corresponding value of 1.65 Å shown in Figure 10 of ref 13.

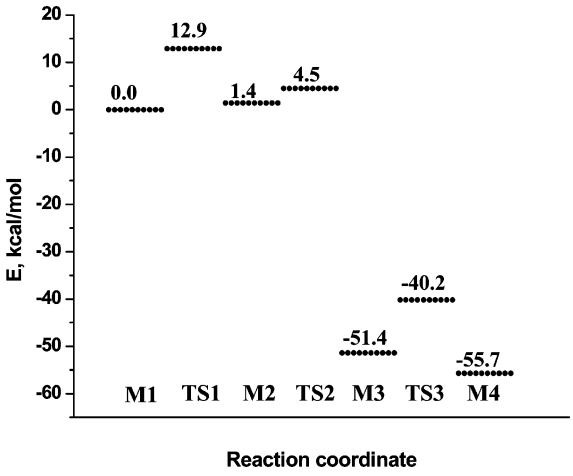

Figure 7. Energy profile calculated for oxygen activation by the iron-containing enzyme.

step and two transition states (the first one resembling our TS3) for the O−O cleavage. One possible explanaition for these differences is the exclusion of the CO_2 moiety from previous calculations.[13] Nevertheless, the overall agreement of the energetics, as well as the general description of the stationary points in the two approaches, is remarkable.

Comparison of Reaction Parameters with Iron, Nickel, and Cobalt in Active Sites

The modeling of the reaction route with the iron in the active site allowed us to repeat the calculations of the stationary points for the corresponding potential surfaces of the active site following Fe^{2+} substitution by Ni^{2+} or Co^{2+}. As in the case of iron-containing site, we tested several possible spin states for the metal site−oxygen molecule complexes by using the B3LYP/LANL2DZdp approximation. The lowest energy structures of the noninteracting moieties corresponded to $S = 2$ (quintet) for nickel and $S = 5/2$ (sextet) for cobalt. However, pilot calculations for the subsequent points on the reaction routes (TS1, M2, TS2, M3, TS3, M4) showed that the lower spin states ($S = 1$ for Ni, and $S = 3/2$ for Co) should be considered for calculations of energy profiles. As for iron, the products of the reaction must correspond to the lower spin state of the system

TABLE 1: Selected Parameters of Transition State TS1 for the Stage of Attachment of Activated Oxygen to 2OG

parameter	Fe	Ni	Co
oxygen−carbon distance in 2OG R(C−O), Å	1.90	1.97	1.92
frequency ω, cm^{-1}	416i	377i	405i
oxygen−oxygen distance R(O_1−O_2), Å	1.28	1.27	1.27
oxygen−metal distance R(O_1−Met), Å	2.09	2.22	2.26
energy counted from M1, kcal/mol	12.9	12.1	15.1

TABLE 2: Selected Parameters of Transition State TS2 for Cleavage of the C−C Bond in 2OG

parameter	Fe	Ni	Co
C−C bond distance in 2OG R(C−C), Å	1.71	1.59	1.63
frequency ω, cm^{-1}	474i	576i	760i
oxygen−carbon distance in 2OG R(C−O_2), Å	1.46	1.59	1.57
oxygen−oxygen distance R(O_1−O_2), Å	1.36	1.31	1.31
oxygen−metal distance R(O_1−Met), Å	2.05	2.31	2.37
energy counted from M1, kcal/mol	4.5	17.8	18.1

compared to the reagents with the triplet-state dioxygen molecule. Apparently, spin crossing should occur on the routes as for the iron site. At points of the first minimum, M1, the energy gap between the high-spin (lower energies) and low-spin states were computed as 9.4 kcal/mol for nickel and 13.1 kcal/mol for cobalt. These values are comparable to the amount 10.7 kcal/mol found for iron. We can partly attribute the differences on the order of 10 kcal/mol between the high-spin and low-spin states in the entrance channel to the DFT methodology. In related articles[20,21] we considered binding of molecular oxygen to the iron-containing sites by using the CASSCF method. The CASSCF calculations with a strict control of populations of d-orbitals on the metal ion resulted in the conclusion that the high-spin ($S = 3$) and low-spin ($S = 2$) energies at the point M1 were almost degenerate. It is reasonable to assume that the same scenario takes place for the nickel and cobalt sites.

For both ions nickel and cobalt the same sets of minima (M1, M2, M3, M4) and transition state structures (TS1, TS2, TS3) were found as for iron. Certain changes in equilibrium geometry configurations as well as in vibrational frequencies were noticed for the different metals, but qualitatively the structures were the same. Atomic coordinates of every stationary point found in this work are given in the Supporting Information.

We report here only the differences in transition states since they are important for the qualitative conclusions. The first transition state TS1 corresponds to the stage of attachment of activated oxygen to the 2OG molecule, as illustrated in Figure 2. In Table 1 we compare the equilibrium distances at respective stationary points for the four-atom motif C(2OG)−O−O−Met, the imaginary harmonic frequencies, and the energies counted from the first minimum point, M1. The activation barrier for the cobalt site is slightly higher than that for iron and nickel; however, the differences between metals do not seem to be substantial for TS1.

Table 2 summarizes the data for the transition state TS2, including the equilibrium distances for the five-atom motif C(2OG)−C(2OG)−O−O−Met (see Figure 3), the imaginary harmonic frequencies, and the energies again counted from the first minimum point, M1. At this stage the differences between metals are noticeable. The lowest energy, referring to iron, correlates well with the longest C(2OG)−C(2OG) distance in 2OG, the least curvature of the saddle point, the largest O−O distance, and the shortest C−O_2 bond length.

The data in Table 3 represent parameters of the third transition state TS3 including distances in the motif C(Sc)−O−Met, imaginary frequencies, and relative energies for this stage of

TABLE 3: Selected Parameters of Transition State TS3 for Cleavage of the O−O Bond in Dioxygen

parameter	Fe	Ni	Co
oxygen−oxygen distance R(O_1−O_2), Å	1.75	2.04	1.98
frequency ω, cm^{-1}	536i	870i	106i
oxygen−carbon distance in Sc R(O_2−C), Å	1.29	1.26	1.28
oxygen−metal distance R(O_1−Met), Å	1.81	1.80	1.69
energy counted from M3, kcal/mol	11.2	30.1	27.4

TABLE 4: Relative Free Energies (kcal/mol) of Critical Points along the Reaction Path in Dioxygen Activation at the Fe, Ni, and Co Metal Sites

point	Fe	Ni	Co
M1	0.0	0.0	0.0
TS1	15.1	19.4	24.4
M2	1.2	−2.4	22.0
TS2	7.6	26.1	28.4
M3	−52.2	−49.5	−51.1
TS3	−42.9	−22.0	−19.2
M4	−54.8	−23.5	−41.6

reaction. Again, the iron-containing active site is characterized by the lowest activation barrier.

Table 4 provides comparison of relative free energies (kilocalories per mole) for all critical points of the overall reaction route for the three different metal-containing enzymes. The solvent corrections (active site environment) are included by using the self-consistent reaction field method as implemented in the Jaguar program system.[19] In the solvation calculations a dielectric constant of 4 and a probe radius of 1.53 Å were assumed. The thermal corrections were calculated for the temperature of 298.15 K.

As one can see, the activation barriers are different in every case. The lowest energy to activate molecular oxygen is required for the iron-containing site (15.1 kcal/mol), and this amount refers to the first transition state TS1. In the cases of nickel and cobalt the rate-limiting step is the stage corresponding to the second transition state TS2 with activation energy of 26.1 and 28.4 kcal/mol, respectively. Such an increase of the reaction barrier of more than 10 kcal/mol may be the reason for inefficiency of possible enzymatic systems in which the parent iron is substituted by nickel or cobalt.

Conclusion

This study presents the results of modeling of the reaction route for molecular oxygen activation by 2OG-dependent hydroxylases containing iron, nickel, or cobalt in the same ligand shell. These calculations are in agreement with the previously obtained data for enzymes with iron-containing sites.[13] Both results are consistent with experimental studies on the non-heme oxygenases or related biomodeled complexes.[11]

The substitution of the iron by nickel or cobalt in the hydroxylase, should such an event occur, may not modify the reaction flow for the coupled oxygen activation and 2OG decarboxylation, or redirect it to a new pathway. The latter possibility was discussed, e.g., in the study of Al-Mjeni et al.[8] Although the calculations do not predict the probability of iron substitution by nickel and/or cobalt ions under physiological conditions, our results clearly demonstrate that these substitutions should slow the reaction by many orders of magnitude. The inefficiency of probable enzymes with nickel or cobalt species in place of iron will be related to considerably higher activation barriers than that for native iron-containing enzymatic systems.

Acknowledgment. A.V.N. thanks the Russian Foundation for Basic Research (Grant 04-03-32007) for partial support of this work. We thank the staff and administration of the Advanced Biomedical Computing Center for their support of this project. This project has been funded in whole or in part with federal funds from the National Cancer Institute, National Institutes of Health, under Contract No. NO1-CO-12400. The content of this publication does not necessarily reflect the views or policies of the Department of Health and Human Services, nor does mention of trade names, commercial products, or organizations imply endorsement by the U.S. Government.

Supporting Information Available: Cartesian coordinates of the computed structures and corresponding spin densities. This material is available free of charge via the Internet at http://pubs.acs.org.

References and Notes

(1) Ivan, M.; Kondo, K.; Yang, H.; Kim, W.; Valiando, J.; Ohh, M.; Salic, A.; Asara, J. M.; Lane, W. S.; Kaelin, W. G., Jr. *Science* **2001**, *292*, 464.

(2) Jaakkola, P.; Mole, D. R.; Tian, Y. M.; Wilson, M. I.; Gielbert, J.; Gaskell, S. J.; Kriegsheim, A.; Hebestreit, H. F.; Mukherji, M.; Schofield, C. J.; Maxwell, P. H.; Pugh, C. W.; Ratcliffe, P. J. *Science* **2001**, *292*, 468..

(3) Lando, D.; Peet, D. J.; Gorman, J. J.; Whelan, D. A.; Whitelaw, M. L.; Bruick, R. K. *Genes Dev.* **2002**, *16*, 1466.

(4) Maxwell, P.; Salnikow, K. *Cancer Biol. Ther.* **2004**, *3*, 29.

(5) Hewitson, K. S.; McNeill, L. A.; Schofield, C. J. *Curr. Pharm. Des.* **2004**, *10*, 821.

(6) Salnikow, K.; Donald, S. P.; Bruick, R. K.; Zhitkovich, A.; Phang, J. M.; Kasprzak, K. S. *J. Biol. Chem.* **2004**, *279*, 40337.

(7) Kovacs, J. A. *Chem. Rev.* **2004**, *104*, 825.

(8) Al-Mjeni, F.; Ju, T.; Pochapsky, T. C.; Maroney, M. J. *Biochemistry* **2002**, *41*, 6761.

(9) Dann, C. E., III; Bruick, R. K.; Deisenhofer, J. *Proc. Natl. Acad. Sci. U.S.A.* **2002**, *99*, 15351.

(10) Elkins, J. M.; Hewitson, K. S.; McNeil, L. A.; Seibel, J. F.; Schlemminger, I.; Pugh, C. W.; Ratcliffe P. J.; Schofield, C. J. *J. Biol. Chem.* **2003**, *278*, 1802.

(11) Costas, M.; Mehn, M. P.; Jemsen, M. P.; Que, L. *Chem. Rev.* **2004**, *104*, 939.

(12) Abu-Omar, M. M.; Loaiza, A.; Hontzeas, N. *Chem. Rev.* **2005**, *105*, 2227.

(13) Borowski, T.; Bassan, A.; Siegbahn, P. E. M. *Chem.*—Eur. J. **2003**, *10*, 1031.

(14) Borowski, T.; Bassan, A.; Siegbahn, P. E. M. *Inorg. Chem.* **2004**, *43*, 3277.

(15) Borowski, T.; Bassan, A.; Siegbahn, P. E. M. *Biochemistry* **2004**, *43*, 12331.

(16) Hay, P. J.; Wadt, W. R. *J. Chem. Phys.* **1985**, *82*, 284.

(17) Frisch, M. J.; Trucks, G. W.; Schlegel, H. B.; Scuseria, G. E.; Robb, M. A.; Cheeseman, J. R.; Montgomery, J. A., Jr.; Vreven, T.; Kudin, J. C.; Burant, J. C.; et al. *Gaussian 03*, Revision B.04; Gaussian, Inc.: Pittsburgh, PA, 2003.

(18) Siegbahn, P. E. M.; Haeffner, F. *J. Am. Chem. Soc.* **2004**, *126*, 8919.

(19) *Jaguar 6.0*; Schrodinger, LLC: Portland, OR, 2005.

(20) Nemukhin, A. V.; Grigorenko, B. L.; Topol, I. A.; Burt, S. K. *Int. J. Quantum Chem.* posted on-line January 5, 2006.

(21) Nemukhin, A. V.; Topol, I. A.; Cachau, R. E.; Burt, S. K. *Theor. Chem. Acc.* **2006**, in press, posted on-line Dec 10, 2005.